

Inhibiting circ_0000673 blocks the progression of colorectal cancer through downregulating CPSF6 via targeting miR-548b-3p

*Shuang Li^{1,A}, *Tuoyun Yang^{2,B}, Lu Liu^{1,C}, Baorong Hu^{1,D}, Xi Chen^{1,D}, Wenting Zhao^{1,E}, Xin Hai^{1,F}

¹ Department of Pharmacy, The First Affiliated Hospital of Harbin Medical University, China

² Department of Critical Care Medicine, The Second Affiliated Hospital of Harbin Medical University, China

A – research concept and design; B – collection and/or assembly of data; C – data analysis and interpretation;

D – writing the article; E – critical revision of the article; F – final approval of the article

Advances in Clinical and Experimental Medicine, ISSN 1899–5276 (print), ISSN 2451–2680 (online)

Adv Clin Exp Med. 2025;34(2):243–255

Address for correspondence

Xin Hai

E-mail: xinhaihu@outlook.com

Funding sources

None declared

Conflict of interest

None declared

*Shuang Li and Tuoyun Yang contributed equally to this work.

Received on June 23, 2023

Reviewed on December 28, 2023

Accepted on March 25, 2024

Published online on September 3, 2024

Abstract

Background. Colorectal cancer (CRC) is one of the most common cancers, and its progression is regulated by several factors, including circular RNA (circRNA).

Objectives. The objective of this study was to determine the role, or roles, of circ_0000673 in CRC.

Materials and methods. We used quantitative real-time polymerase chain reaction (qPCR) to detect the expression of circ_0000673, miR-548b-3p and cleavage and polyadenylation specific factor 6 (CPSF6) in DLD-1 and RKO cells. Cell Counting Kit-8 (CCK-8) and 5-ethynyl-2'-deoxyuridine (EdU) assays were used to determine circ_0000673 roles in proliferation. Wound healing and transwell assays were used to detect cell migration and invasion abilities. Expression of CPSF6 protein and stem cell-associated proteins were examined using western blot. The putative relationship between miR-548b-3p and circ_0000673 or CPSF6 was verified with dual-luciferase reporter assay. The role of circ_0000673 in CRC was also investigated in a tumor xenograft assay in nude mice.

Results. Circ_0000673 expression was increased in CRC tissues and cancer cells. Silencing circ_0000673 reduced tumor cell proliferation, migration and invasion, while also decreasing cell stemness. MiR-548b-3p was found to be a target of circ_0000673, while CPSF6 was a downstream target of miR-548b-3p. The tumor-regulatory effects of si-circ_0000673, anti-miR-548b-3p and oe-CPSF6 were partially reversed by anti-miR-548b-3p, si-CPSF6 and si-circ_0000673, respectively, in rescue assays. Downregulation of circ_0000673 reduced solid tumor growth in vivo.

Conclusions. Circ_0000673 inhibition reduced CPSF6 expression by targeting miR-548b-3p, thereby blocking proliferation, migration and invasion of CRC tumor cells.

Key words: colorectal cancer, CPSF6, circ_0000673, miR-548b-3p

Cite as

Shuang Li, Yang T, Liu L, et al. Inhibiting circ_0000673 blocks the progression of colorectal cancer through downregulating CPSF6 via targeting miR-548b-3p. *Adv Clin Exp Med.* 2025;34(2):243–255. doi:10.17219/acem/186500

DOI

10.17219/acem/186500

Copyright

Copyright by Author(s)

This is an article distributed under the terms of the Creative Commons Attribution 3.0 Unported (CC BY 3.0) (<https://creativecommons.org/licenses/by/3.0/>)

Background

Progression of colorectal cancer (CRC) begins with abnormal transformation of epithelial cells in the colon or rectum and has the 3rd highest incidence and 2nd highest mortality rate of all malignancies.^{1,2} In developing countries, the incidence of CRC is quickly growing and is now more than 4 times that of industrialized countries.³ Moreover, the prognosis for individuals with advanced CRC remains poor, with recurrence and distant metastases being the primary causes of death following surgery.^{4,5} The mechanism of CRC carcinogenesis is complex and entails numerous steps in the disease evolution. Numerous genes and signaling pathways have been implicated in tumor cell invasion and metastasis, yet the underlying mechanisms of CRC are not thoroughly understood. Thus, exploring the molecular pathways integral to the pathogenesis of CRC and identifying novel biomarkers are pivotal for enhancing early diagnosis and prognosis for patients.

Circular RNA (circRNA), a type of non-coding RNA, possesses a covalently closed-loop structure at the 3' and 5' untranslated regions (UTRs), resulting from the reverse splicing of precursor messenger RNA (pre-mRNA).^{6–8} Circular RNA is more stable than linear RNA in cells due to its unique structure, which prevents cleavage from exonucleases. Circular RNA is involved in various aspects of cancer biology and can play a crucial role in regulating gene expression by acting as a sponge for microRNAs (miRNAs).^{9–11} It is also linked to malignant tumor characteristics, including cell proliferation, the cell cycle and invasion. For instance, silencing of circ_RNF121 can reduce cell proliferation, metastasis and glycolysis through the miR-1224-5p/*FOXMI* axis, which plays a significant role in CRC progression.¹² Circ-LECRC functions as a competitive endogenous RNA (ceRNA) to regulate *KLF4* expression and acts as a “brake signal” to reduce the over-activation of oncogenic *YAP* signaling, thereby inhibiting CRC tumor growth.¹³ However, whether circ_0000673 plays a role or participates in particular mechanisms in CRC requires further research.

Objectives

By conducting an extensive review of existing literature and conducting meticulous bioinformatics analysis, our goal was to explore the potential significance of circ_0000673 as a pivotal circRNA in the regulation of CRC progression, specifically through the miR-548b-3p/*CPSF6* pathway. Unraveling these intricate molecular mechanisms in the context of CRC tumorigenesis not only enhances our comprehension but also sets the stage for potential clinical applications in this domain.

Materials and methods

Tissues collection and study approval

A cohort of 34 CRC patients was enlisted from the Second Affiliated Hospital of Harbin Medical University, China, for this study. The resected tissues were immediately preserved in liquid nitrogen for RNA analysis. Pathological sections confirmed that all tumor tissues belonged to CRC, and the patients' clinicopathological information was fully documented. Informed consent forms were signed by all patients or their family members, indicating their awareness and approval of sample usage. The collection of clinical specimens was conducted in accordance with the ethical standards set forth by the Ethics Committee of the Second Affiliated Hospital of Harbin Medical University (approval No. KY2021-230).

Cell culture

The CRC cell lines DLD-1 and RKO, alongside the normal colorectal epithelial cell lines NCM460, were procured from the Institute of Type Culture, Chinese Academy of Sciences, Shanghai, China. After retrieving the frozen storage tube from liquid nitrogen, it was immediately thawed in a water bath at 37°C to ensure rapid lysis. The contents were then transferred to an ultra-clean operating table for further processing. Initially, the cell suspension was pipetted from the freezing tube into a 15 mL centrifuge tube, and 1 mL of complete culture medium was added and mixed. The mixture was then centrifuged at 1,000 rpm for 5 min, and the supernatant was carefully decanted. Subsequently, 5 mL of complete medium was added to the centrifuge tube, and the cells were gently mixed and transferred to cell culture dishes or flasks. The cells were finally incubated in an incubator at 37°C with 5% CO₂. All cells were maintained for less than 6 months.

Quantitative real-time polymerase chain reaction

Cells were lysed and centrifuged, and the precipitated material was transferred to a centrifuge tube and centrifuged at 1,000 rpm for another 5 min, after which the supernatant was discarded, and TRIzol (Invitrogen, Waltham, USA; 15596026) reagent was added to the pellet. The solution was then gently mixed several times to rupture the cells and shear the DNA. The Reverse Transcription Kit (Roche, Penzberg, Germany; 11483188001) was then used to generate complementary DNA (cDNA). The PCR system with FastStart Universal SYBR Green master (Roche; FSSGMMRO) and a C1000 thermal cycler were used to perform quantitative real-time polymerase chain reaction (qPCR). Internal controls were *GAPDH* and *U6*, and the data were evaluated using the 2^{−ΔΔCt} technique.¹⁴ All primer sequences are listed in Supplementary Table 1.

Cell transfection

To perform cell transfection, 125 μL of serum-free Dulbecco's modified Eagle's medium (DMEM) was added to each Eppendorf (EP) tube and labeled accordingly. Next, 5 μL of Lipofectamine 3000 (Invitrogen; V518472) was added along with 5 μL of diluted siRNA to each of the 2 EP tubes. The contents of the EP tubes were mixed thoroughly by gentle pipetting to homogenize and then allowed to stand at room temperature for 15 min. When the cells reached 40–60% confluency, the supernatant was discarded, and the cells were washed twice with sterile phosphate-buffered saline (PBS). Next, the serum-free DMEM medium was added to the cells, and then the mixture from the EP tubes was put into the corresponding well of the 6-well plate. The contents were mixed well, and the plate was placed in the incubator for further cultivation. After 6–8 h, the medium was replaced with complete medium. To detect the RNA content, transient transfection was performed for 48–72 h, and for protein content and functional experiments, it was performed for 72 h.

Ribonuclease R (RNase R) and actinomycin D treatment

The loop structure of circ_0000673 was confirmed via RNase R treatment. A total of 5 μg of RNA, extracted from DLD-1 and RKO cells, was treated with 2 U/ μg of RNase R (Genesee, Guangzhou, China; R0301) at 37°C for 30 min. Subsequently, the enzyme was inactivated at 70°C for 5 min. DEPC-treated water (MilliporeSigma, St. Louis, USA) served as a control. Actinomycin D (2 $\mu\text{g}/\text{mL}$) or dimethyl sulfoxide (DMSO; MilliporeSigma; D2650-100ML) were introduced to media containing DLD-1 or RKO cells for 0, 4, 8, and 12 h to analyze actinomycin D disposal. Then, we used qPCR to detect the expression of circ_0000673 and corresponding linear RNA.

Cell Counting Kit-8 assay

Colorectal cancer cells post-transfection were grown in 96-well plates with a density of 1×10^5 cells per well. At each designated time point (0, 24, 48, and 72 h), 10 μL of Cell Counting Kit-8 (CCK-8) reagent (Beyotime Biotechnology, Shanghai, China; C0037) was incorporated per well and then incubated for an additional 2 h at 37°C within a humidified incubator. Finally, the absorbance at 450 nm was read using a microplate reader (iMark; Bio-Rad, Hercules, USA).

5-ethynyl-2'-deoxyuridine assay

The target cell line in logarithmic growth was selected, and a cell suspension was prepared. The cells were inoculated into a 96-well plate, and 100 μL of diluted

5-ethynyl-2'-deoxyuridine (EdU) in complete medium (50 μM) (Beyotime Biotechnology; C0071S) was added and incubated for 2 h. In the dark, cells were subjected to flow incubation, fixed with 4% paraformaldehyde, and successively treated with permeabilizing solution, Click-Interaction mixture and fluorescent nuclear stains. After each treatment, cells were washed with an immunostaining blocking buffer. Finally, images of the cells were captured using a fluorescent microscope (Leica DMI4000 B; Leica Camera AG, Wetzlar, Germany) and the cells were counted with different fluorescent colors.

Transwell assay

The cells to be treated were initially resuspended in serum-free medium. Subsequently, cell counting was performed, and the cells were appropriately diluted to obtain a concentration of $1 \times 10^5/\text{mL}$. Then, 200 μL of the cell suspension was aspirated and added dropwise to the upper chamber of the transwell. Following this, complete medium (0.7 mL) was added to the lower chamber. For invasion experiments, a diluted layer of Matrigel (BD Biosciences, San Jose, USA; 353095) was applied to the surface of the chambers. After a 24-h incubation period, the underlying cells were fixed for 30 min with 4% paraformaldehyde and stained for 1 h with 0.5% crystal violet. Finally, images were acquired using an inverted optical microscope (Leica DMI4000 B) and the quantity of migrating or invading labeled cells was counted using ImageJ software (National Institutes of Health (NIH), Bethesda, USA).

Wound healing assay

DLD-1 and RKO cells were seeded at a density of 6×10^5 per well in 6-well plates and allowed to grow for 48 h. Once 90% confluence was achieved, a linear scratch was made in each well using a 200 μL pipette tip. Then, cells were washed in PBS and incubated in complete medium. After 24 h of incubation, the width of the wound was analyzed.

Spheroid formation assay

Spheroid formation assay was performed in serum-free medium supplemented with $\times 1$ B27, 20 ng/mL each of epidermal growth factor (EGF) and basic fibroblast growth factor (bFGF, Invitrogen; 17504-044, 266775, 266475), along with 100 U/mL penicillin and 0.1 mg/mL streptomycin (Beyotime Biotechnology; c0222) and required special ultra-low attachment plates (Corning Company, Corning, USA; 7007). The quantity and size of spheroids were measured using an inverted optical microscope (Leica DMI4000 B) after 10 days. The efficiency of spheroid formation was calculated using the formula as the number of colonies divided by the number of seeded cells.

Dual-luciferase reporter assay

The binding sequence of circ_0000673 or *CPSF6* to miR-548b-3p was predicted, and genomic DNA from CRC cells was extracted and amplified. The double-enzymatic luciferase reporter gene empty plasmid used was pGL3 (Promega, Madison, USA). The luciferase reporter vector generated (pmirGLO-circ_0000673-WT, pmirGLO-circ_0000673-MUT, pmirGLO-*CPSF6*-WT, pmirGLO-*CPSF6*-MUT) and miR-NC or miR-548b-3p mimics were co-transfected into DLD-1 and RKO cells. Luciferase activity was detected using the dual-luciferase reporter detection system kit (Promega; E1910) after transfection for 48 h.

Western blot assay

After lysing cells or tissues with RIPA Lysis Buffer (Beyotime Biotechnology; P0013B) and 1% phenylmethylsulfonyl fluoride (PMSF) (Seven, Beijing, China; SW106) to collect proteins, the protein concentration was determined using the BCA Protein Concentration Assay Kit (Beyotime Biotechnology; P0009), and the proteins subjected to sodium dodecyl sulfate-polyacrylamide gel electrophoresis (SDS-PAGE). Proteins on polyacrylamide gels were subsequently transferred to polyvinylidene difluoride (PVDF) membranes (Millipore, Billerica, USA) using electrophoretic techniques. The PVDF membranes were sealed with a sealing solution at room temperature for a period adjusted for the different antibodies, followed by overnight incubation at 4°C in a cold room immersed in primary antibody. The next day the membranes were washed 3 times with phosphate-buffered saline with Tween (PBST) and then incubated with the secondary antibody for 1.5 h at room temperature and washed again in PBST. The expression level of the target protein was assessed using a BeyoECL kit (Beyotime Biotechnology; P0018S), with glyceraldehyde

3-phosphate dehydrogenase (GAPDH) serving as an internal reference. All antibodies were sourced from Immunoway (Texas-Plano, USA; NESTIN: YN2050, SOX2: YM0594) or Abcam (Cambridge, USA; CPSF: ab175237, OCT4: ab200834). The antibody was diluted in accordance with the manufacturer's instructions.

Xenograft assay

We purchased nude BALB/c mice from Vital River (Beijing, China) and housed them in a barrier system at 45–50% humidity and 25–27°C. A CRC xenograft model was established by subcutaneously injecting $5 \times 10^6/150 \mu\text{L}$ of transfected CRC tumor cells into the anterolateral groin of the left hind limb and $5 \times 10^6/150 \mu\text{L}$ of sh-NC transfected tumor cells into the anterolateral groin of the right hind limb of each mouse. Tumor volume was measured once a week. After 4 weeks, the mice were euthanized by cervical dislocation, and the tumors were dissected and weighed, and the expression of genes under study was also assessed. The Ethics Committee of The Second Affiliated Hospital of Harbin Medical University approved the study (approval No. SYDW2021-052).

Statistical analyses

The data were analyzed using IBM SPSS v. 27.0 (IBM Corp., Armonk, USA). Data visualization was performed using GraphPad Prism v. 9 (GraphPad Software, San Diego, USA). Data were expressed as mean \pm standard deviation (\pm SD) and underwent analysis based on the grouping or pairing conditions, employing distinct Mann–Whitney test, Kruskal–Wallis test and post hoc multiple comparisons. The clinicopathologic data in Table 1 were examined using Fisher's exact test. Due to the limited sample size, non-parametric tests were used, leading to marginal

Table 1. Correlation between circ_0000673 expression and clinicopathological characteristics of colorectal cancer (CRC) patients

Clinicopathological characteristics		Total cases (n = 34)	Circ_0000673 expression		p-value
			low (n = 17)	high (n = 17)	
Age [years]	<60	12	5	7	0.360
	≥ 60	22	12	10	
Gender	male	20	11	9	0.364
	female	14	6	8	
Tumor size [cm]	<5	23	13	10	0.232
	≥ 5	11	4	7	
Differentiation grade	well/moderate	17	10	7	0.274
	poor/undifferentiated	17	7	10	
TNM stage	I–II	14	10	4	0.039*
	III–IV	20	7	13	
Lymph node invasion	positive	19	6	13	0.018*
	negative	15	11	4	

*p < 0.05. TNM – tumor-node-metastasis staging system.

significance in the reported results, and the statistical methods and detailed parameters utilized for all results were documented in Supplementary Table 2.

Results

Circ_0000673 was upregulated in CRC tissues and cells

We first identified the basic characteristics of circ_0000673, which is 251 nucleotides in length produced by exons 4 and 5 of *RSL1D1* mRNA (Fig. 1A). To explore the relevance of circ_0000673 to CRC progression, we examined its expression in CRC cells. Quantitative real-time polymerase chain reaction assays pointed to higher circ_0000673 enrichment being detected in CRC cell lines (DLD-1, RKO and HT-29),

compared to NCM460 cells (Fig. 1B). After RNase R treatment, we found that circ_0000673 was resistant to RNase R digestion when compared to *RSL1D1* (Fig. 1C,D). After total RNA synthesis was inhibited by actinomycin D, the expression of circ_0000673 and *RSL1D1* mRNA were detected at different time points, and again, the stability of circRNA was found to be much stronger than that of linear mRNA (Fig. 1E,F).

The relationship between circ_0000673 and clinicopathologic data of CRC patients

Considering the elevated expression of circ_0000673 in CRC tissues compared to normal tissues (Fig. 2A), we investigated the relationship between circ_0000673 expression and the pathological advancement of CRC. Initially, we categorized the patients based on the presence of lymph node metastasis or TNM (tumor-node-metastasis) stage

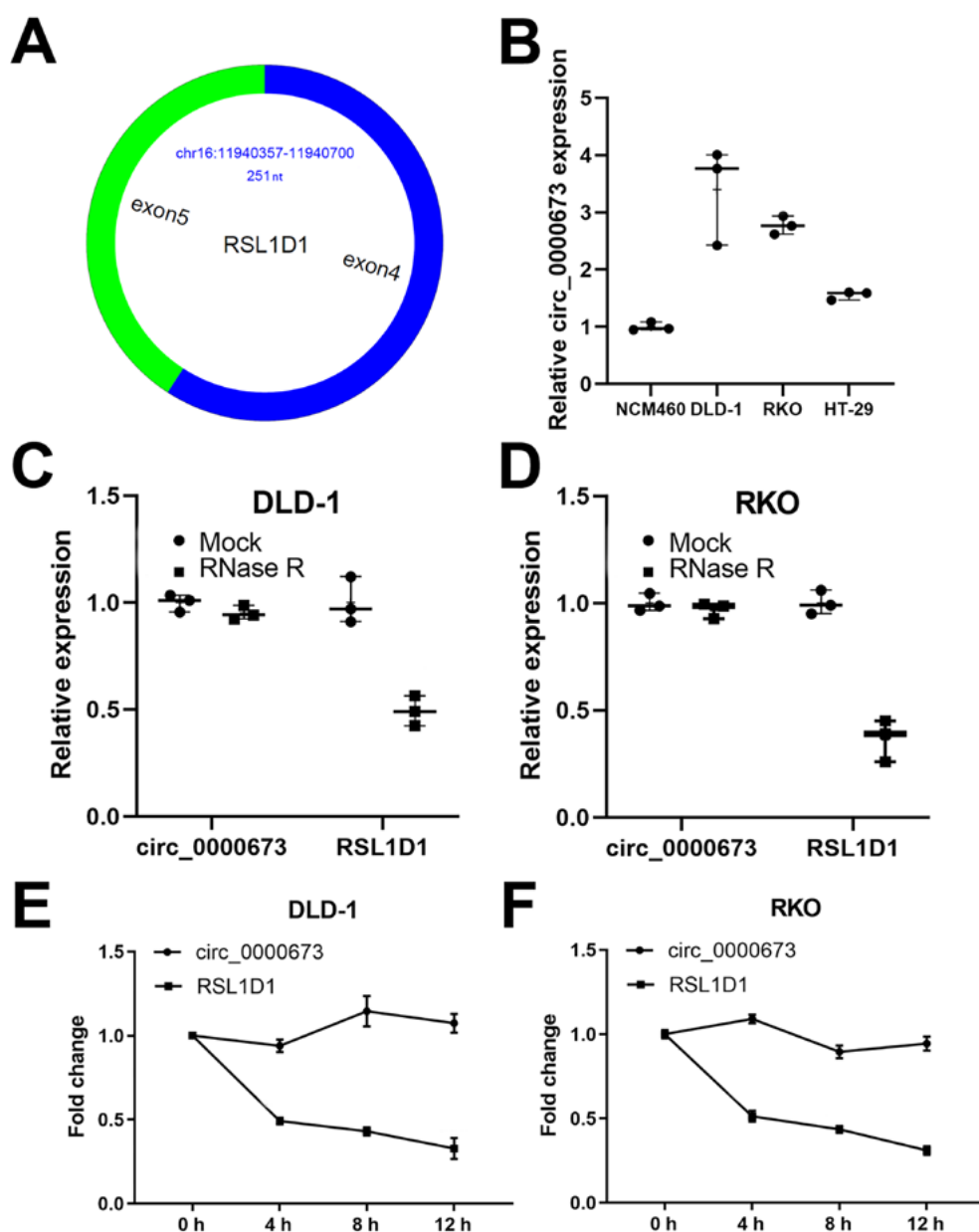


Fig. 1. Circ_0000673 was upregulated in CRC cells.

A. Diagram showing the structure of circ_0000673 derived from *RSL1D1* mRNA; B. qPCR assay was used for the expression of circ_0000673 in NCM460, DLD-1, RKO and HT-29 cells; C,D. The relative circ_0000673 and *RSL1D1* expression were detected using the qPCR in CRC cells treated with RNase R; E,F. Actinomycin D assay in DLD-1 and RKO cells. Kruskal–Wallis test was employed for the comparison of circ_0000673 among different cell types, followed by the Bonferroni post hoc test. The comparison between circ_0000673 and *RSL1D1* was conducted using the Mann–Whitney test

CRC – colorectal cancer;
qPCR – quantitative real-time polymerase chain reaction;
RNase – ribonuclease.

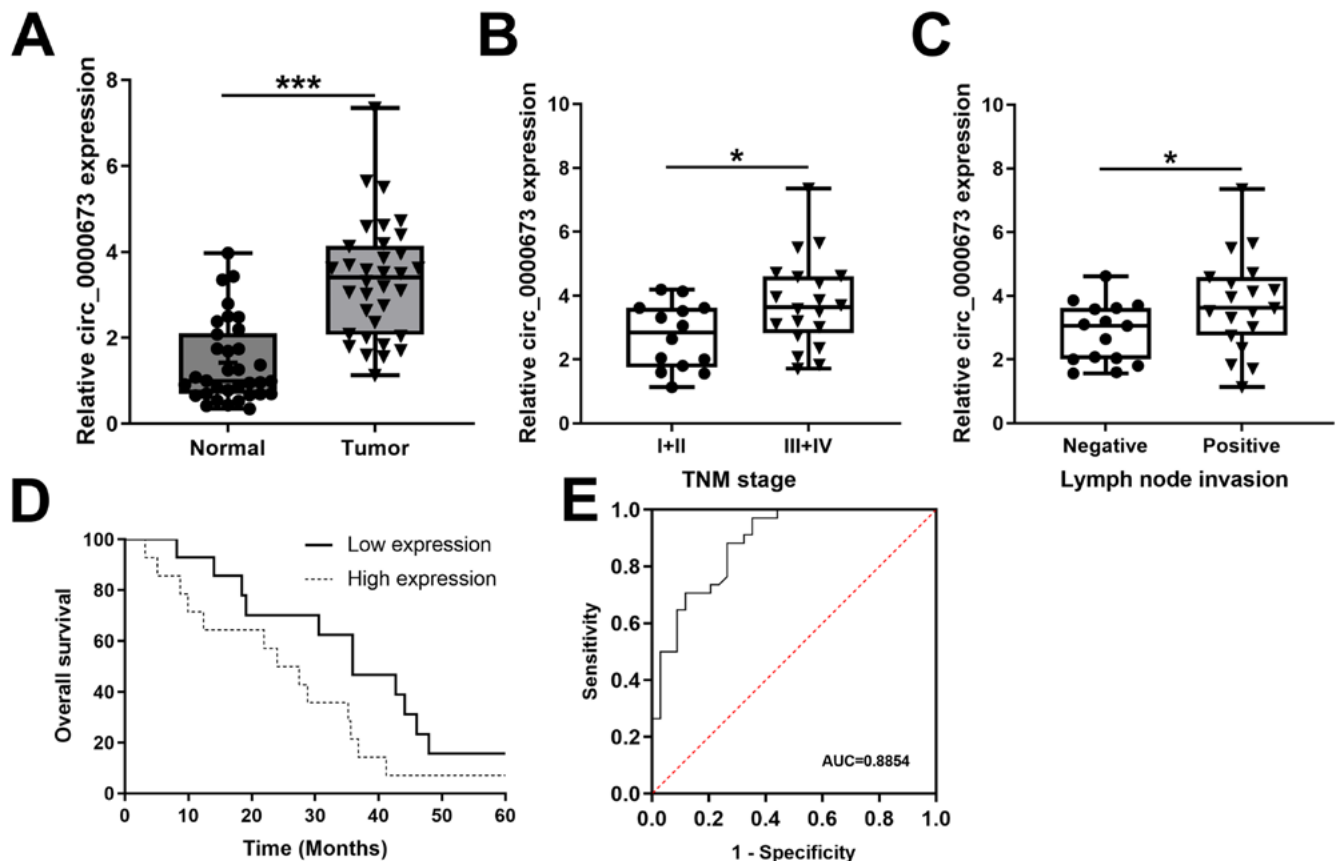


Fig. 2. *Circ_0000673* expression in CRC tissues and its correlation with clinical features and prognosis. A. qPCR assay for the expression of *circ_0000673* in tumor and adjacent normal tissues; B,C. Association of *circ_0000673* expression in patients with TNM stage or presence of lymph node invasion; D. Overall survival (OS) comparison between high and low *circ_0000673* expression groups; E. The ROC curve of *circ_0000673* detection as a prognostic biomarker. The comparison of *circ_0000673* among different tissues and stages was conducted using a paired t-test

* $p < 0.05$, *** $p < 0.001$; CRC – colorectal cancer; qPCR – quantitative real-time polymerase chain reaction; TNM – tumor-node-metastasis staging system; ROC – receiver operating characteristic.

and subsequently performed quantitative comparisons of *circ_0000673* expression levels within each group using qPCR (Fig. 2B,C). However, to explore whether *circ_0000673* could play a role in the clinical setting, we also analyzed its correlation with pathological data after dividing all cases into *circ_0000673* high- and low-expression groups (Table 1). Survival correlation, as analyzed using a Kaplan–Meier estimation, revealed that patients exhibiting high *circ_0000673* expression experienced poorer overall survival (OS) compared to their counterparts with low *circ_0000673* expression (log-rank $p = 0.043$; Fig. 2D). To evaluate the prognostic efficacy of *circ_0000673*, we plotted receiver operating characteristic (ROC) curves, and the results confirmed that *circ_0000673* had clinical prognostic significance ($p < 0.001$; Fig. 2E).

Circ_0000673 downregulation restricted the proliferation, invasion and migration of cancer cells

Once the transfection efficacy of si-*circ_0000673* was assessed (Fig. 3A), CCK-8 and EdU assays revealed

a significant reduction in the vitality of DLD-1 and RKO cells following si-*circ_0000673* transfection compared to the si-NC group (Fig. 3B–D). Building upon the findings presented above, the downregulation of *circ_0000673* exhibits the capacity to curb the proliferation of CRC cells. We extended our investigation to assess the influence of *circ_0000673* on the invasive and migratory capabilities of CRC cells, employing both wound healing and transwell assays. The results indicated that in cells transfected with si-*circ_0000673*, the migration distance of tumor cells and the number of migrating cells were notably lower compared to the control group (Fig. 4A,B). Moreover, the transwell assay showed a reduction in the number of invasive cells in the experimental group following the removal of the stromal gel layer (Fig. 4C). The number of invasive cells in the transwell layer was also reduced (Fig. 4D). A subsequent attenuation of tumor cell stemness after knockdown of *circ_0000673* can be seen in the spheroid formation assay, and some stemness markers like *NESTIN*, *OCT4* and *SOX2* were also downregulated at the protein expression level (Fig. 5A,B).

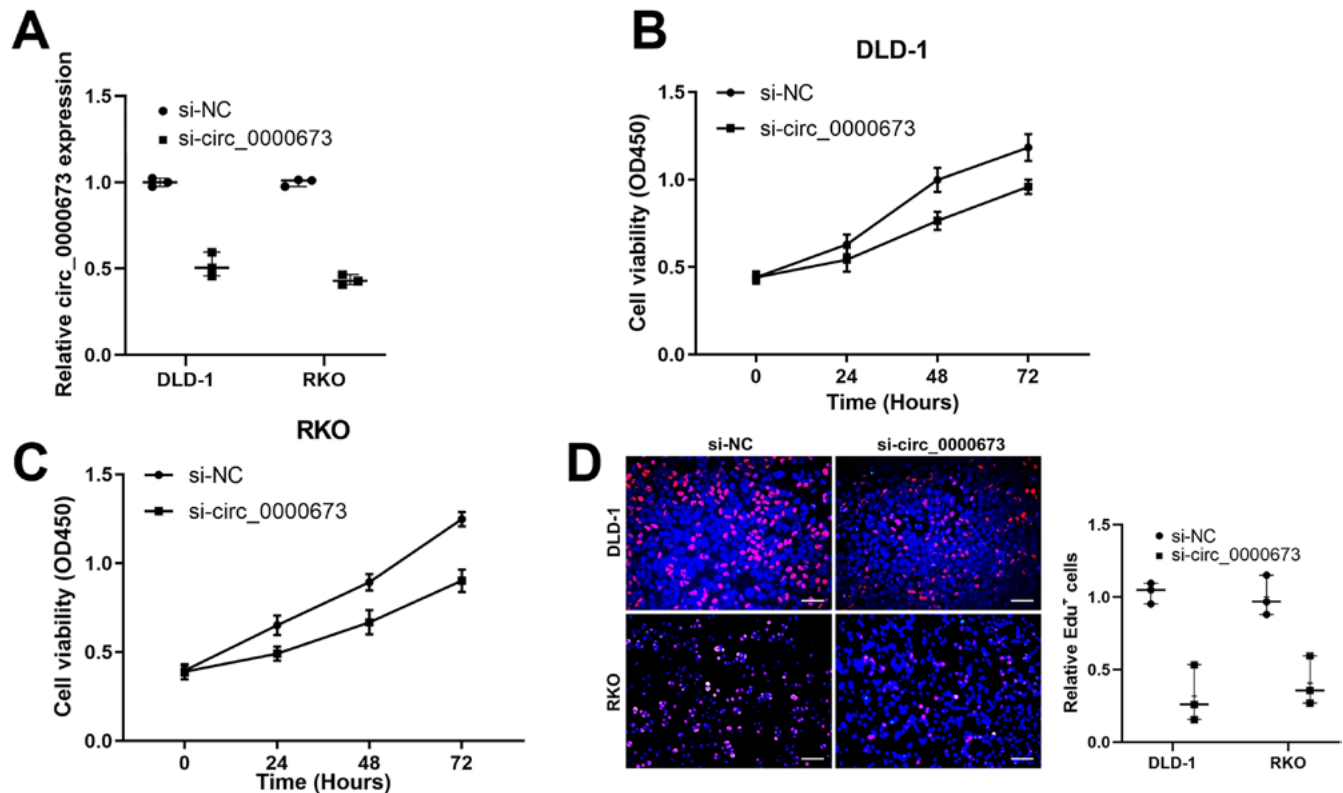


Fig. 3. Downregulation of circ_0000673-inhibited CRC cell proliferation. A. qPCR determined circ_0000673 expression in transfected cells; B,C. CCK-8 assay was performed to examine the cell viability of transfected CRC; D. EdU assay was used to determine cell proliferation. All statistical analyses employed in this figure were performed using the Mann–Whitney test

CRC – colorectal cancer; qPCR – quantitative real-time polymerase chain reaction; CCK-8 – Cell Counting Kit-8; EdU – 5-ethynyl-2'-deoxyuridine.

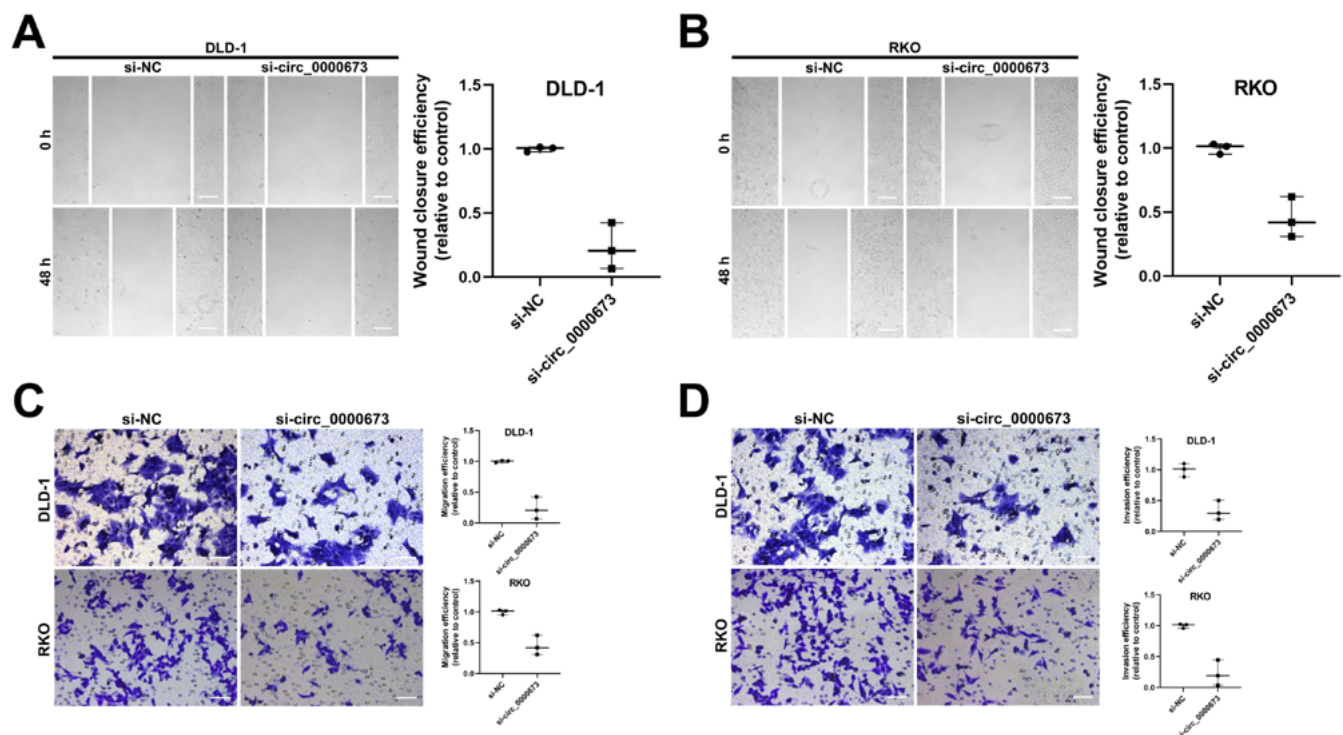


Fig. 4. Knockdown of circ_0000673 expression suppressed migration and invasion in CRC cells. A,B. Wound healing assay was used to detect the migration ability of CRC cells after circ_0000673 knockdown; C,D. Transwell assay gauged cell migration and invasion. All statistical analyses employed in this figure were performed using the Mann–Whitney test

CRC – colorectal cancer.

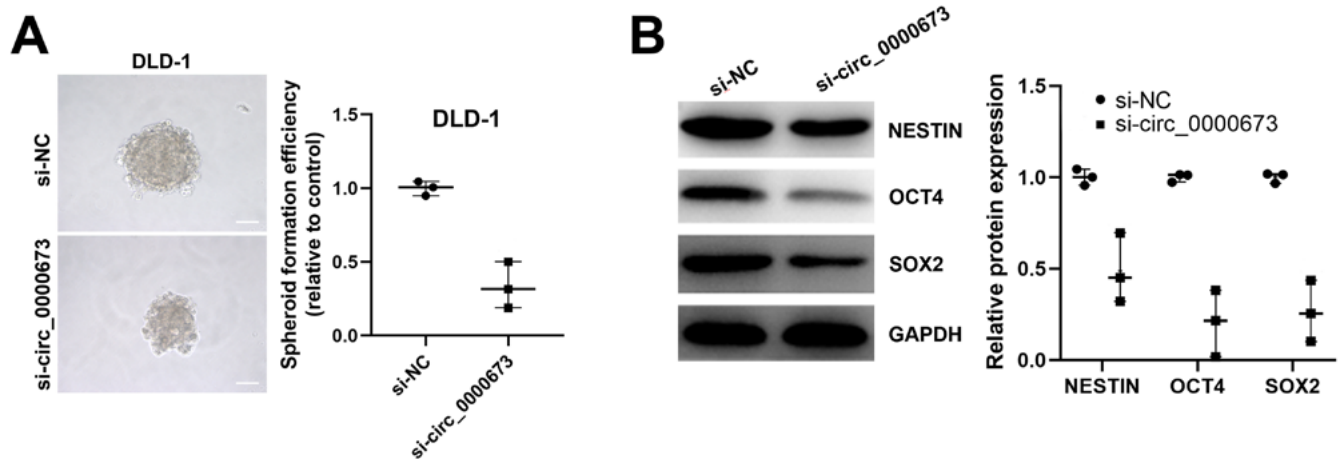


Fig. 5. Inhibited *circ_0000673* could affect tumor cell stemness. **A.** Spheroid formation was used to evaluate the spheroid-forming abilities of transfected DLD-1 cells; **B.** Western blot assay was conducted to analyze the protein expression of NESTIN, OCT4 and SOX2. All statistical analyses employed in this figure were performed using the Mann–Whitney test

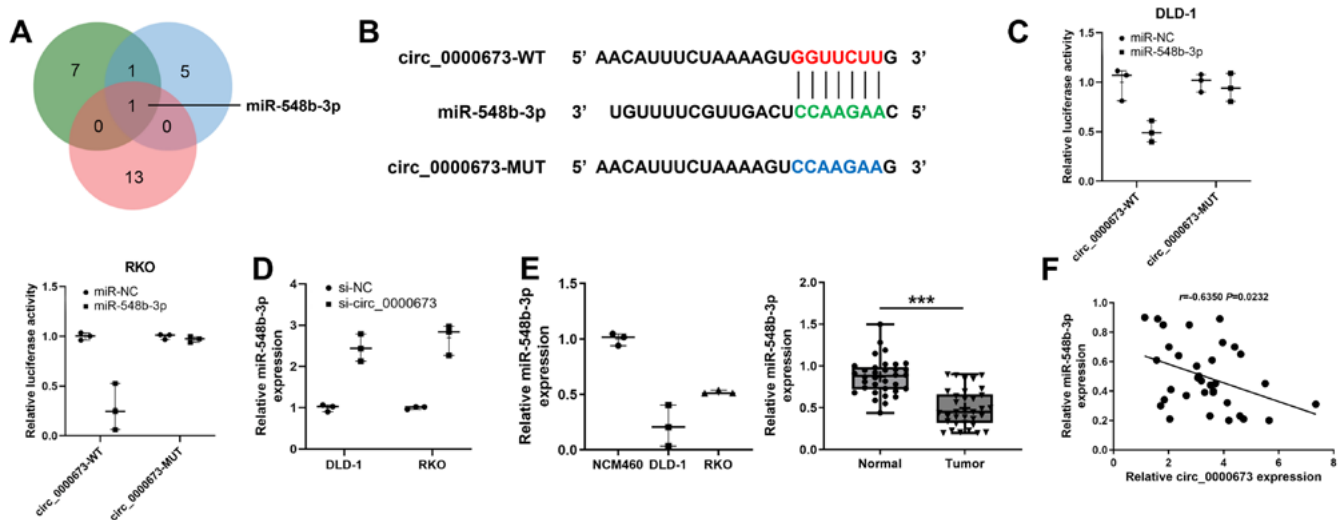


Fig. 6. MiR-548b-3p was a direct target of *circ_0000673*. **A** Venn diagram was used to screen miRNAs targeted *circ_0000673* from circinteractome, Starbase and circBANK; **B.** The binding sets between miR-548b-3p and *circ_0000673* were presented; **C.** Dual-luciferase reporter assay confirmed the miR-548b-3p and *circ_0000673* interaction; **D.** MiR-548b-3p expression in cells transfected with a negative control vector or *circ_0000673* inhibitor was detected using qPCR; **E.** The expression of miR-548b-3p in NCM460, DLD-1 and RKO cells was detected with qPCR. The miR-548b-3p expression in CRC tumor tissues and normal tissues was detected using qPCR; **F.** The correlation between miR-548b-3p and *circ_0000673* expression was analyzed using the Pearson's correlation coefficient. The statistical analysis for the dual-luciferase reporter gene experiment and the differential expression of miR-548b-3p in cells were both assessed using the Mann–Whitney test. The expression differences of miR-548b-3p among different tissues were analyzed using a paired t-test

*** $p < 0.001$; qPCR – quantitative real-time polymerase chain reaction; CRC – colorectal cancer.

Targeted regulation of miR-548b-3p expression by *circ_0000673* in colorectal cancer cells

Circinteractome, starBase and circBANK predicted that miR-548b-3p may act downstream of *circ_0000673* in regulating CRC (Fig. 6A,B). To validate this hypothesis, we conducted a dual-luciferase reporter assay. The experimental results confirmed our hypothesis, showing that the luciferase activity was significantly reduced in DLD-1 and RKO cells co-transfected with miR-548b-3p mimics and the recombinant plasmid *circ_0000673*-WT (Fig. 6C). Using qPCR assay, miR-548b-3p expression level was significantly increased

after transfection with si-*circ_0000673* compared to that with small interfering RNA negative control (si-NC) group (Fig. 6D), and miR-548b-3p expression was found to be downregulated in CRC cells and tissues (Fig. 6E). It is worth noting that the expression of *circ_0000673* and miR-548b-3p in CRC tissues presented a negative relationship (Fig. 6F).

CPSF6 severed as a downstream effector of miR-548b-3p in CRC

Bioinformatics analysis disclosed that miR-548b-3p could target *CPSF6* (Fig. 7A). The results obtained from the experiment indicate that luciferase activity was considerably

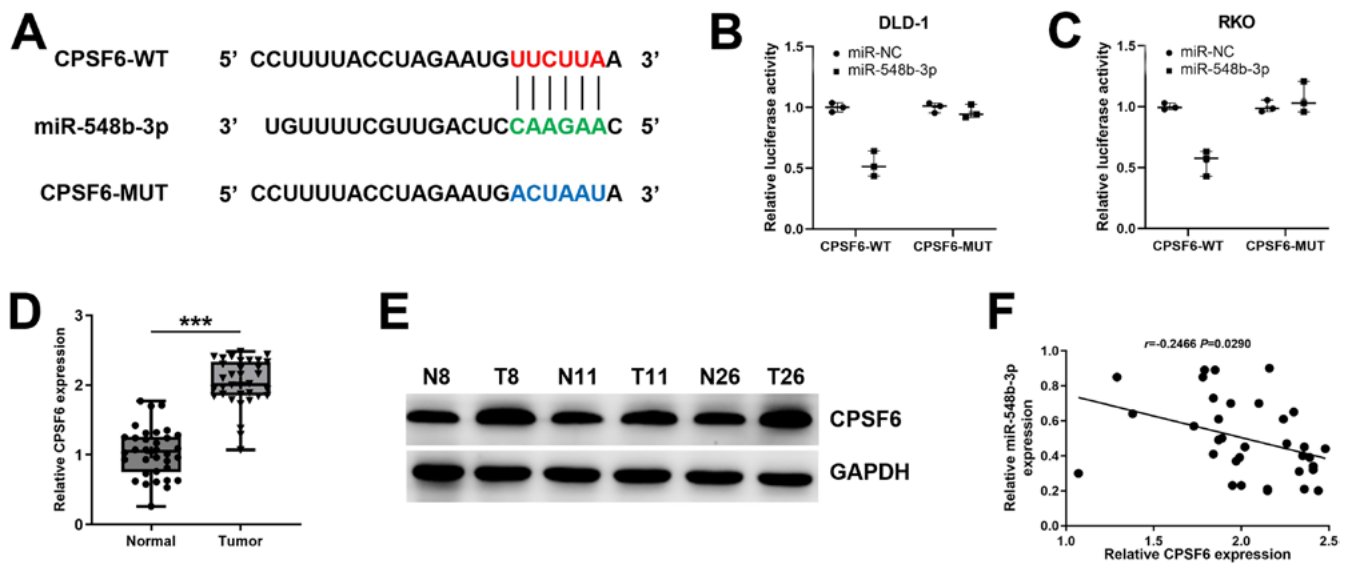


Fig. 7. *CPSF6* was a target gene of miR-548b-3p in CRC tissues. **A**, The binding sets between *CPSF6* and miR-548b-3p were analyzed using Starbase; **B,C**, The relationship between *CPSF6* and miR-548b-3p was validated with dual-luciferase reporter assay; **D,E**, *CPSF6* mRNA and protein expression in normal tissues and CRC tissues were detected using qPCR and western blot, respectively; **F**, The correlation between *CPSF6* mRNA and miR-548b-3p expression was analyzed in CRC tissues. The analysis of the dual-luciferase reporter gene experiment, the regulation of *CPSF6* expression by miR-548b-3p, and the assessment of *CPSF6* tissue protein expression levels were all conducted using the Mann–Whitney test. The mRNA level differences of *CPSF6* between normal and tumor tissues were evaluated using a paired t-test

*** $p < 0.001$; CRC – colorectal cancer.

weaker in the *CPSF6*-WT cells transfected with miR-548b-3p compared with the control group, while the luciferase activity was not significantly changed in the *CPSF6*-MUT group cells transfected with miR-548b-3p mimics (Fig. 7B,C). In CRC tissues, we observed that both *CPSF6* mRNA and protein were increased and *CPSF6* expression was negatively correlated with miR-548b-3p expression (Fig. 7D–F). Similarly, the *CPSF6* nucleic acid and protein expression levels were elevated in CRC cells (DLD-1 and RKO) (Fig. 8A,B). The addition of anti-miR-548b-3p significantly increased *CPSF6* abundance, but miR-548b-3p overexpression decreased *CPSF6* expression (Fig. 8C).

Circ_0000673 regulated CRC malignant biological behaviors via miR-548b-3p/*CPSF6*

We performed rescue experiments to further characterize the regulatory relationship between circ_0000673 and *CPSF6*. It was found that circ_0000673 knockdown suppressed *CPSF6* expression at both the nucleic acid and protein levels, and then rescued *CPSF6* repression by silencing miR-548b-3p in part (Fig. 8D). The findings suggest that circ_0000673 could function as a ceRNA, potentially binding to miR-548b-3p to elevate *CPSF6* in CRC cells. Subsequent rescue experiments regarding cellular phenotype were also conducted. Cell Counting Kit-8 and EdU rescue assays provided further confirmation that the reduced cell proliferation due to circ_0000673 knockdown could be restored by suppressing miR-548b-3p (Fig. 9A–C). Additionally, transwell assays showed that the circ_0000673 knockdown-induced

inhibition of migration and invasion capabilities could be partially reversed by inhibiting miR-548b-3p. Moreover, the downregulation of cell proliferation, migration and invasion by miR-548b-3p was partially mitigated upon transfection with si-*CPSF6* (Fig. 10A–C). Finally, overexpression of *CPSF6* significantly amplified the proliferation, migration and invasion of tumor cells, while the knockdown of circ_0000673 partly countered these effects (Fig. 11A–C). In conclusion, circ_0000673/miR-548b-3p/*CPSF6* axis is involved in the tumorigenic process of CRC.

Circ_0000673 silencing restrains xenograft tumor growth in vivo

A CRC xenograft model was established to confirm the effects of circ_0000673 on CRC tumorigenicity. RKO cells at the logarithmic growth stage were inoculated into nude mice after transfection with sh-circ_0000673 or short hairpin RNA negative control (sh-NC) and monitored for 4 weeks. Both tumor volume and weight of the sh-circ_0000673 transfected group were decreased (Fig. 12A,B), indicating that circ_0000673 silencing was able to inhibit the growth of xenograft tumors in vivo. Quantitative real-time polymerase chain reaction and western blot on tumor tissues showed circ_0000673 expression was severely decreased in sh-circ_0000673 group tumors (Fig. 12C). Conversely, the expression of miR-548b-3p was upregulated due to the silenced circ_0000673 (Fig. 12D). In addition, mRNA and protein expression of *CPSF6* were significantly decreased in sh-circ_0000673 tumor tissues compared to sh-NC group (Fig. 12E,F).

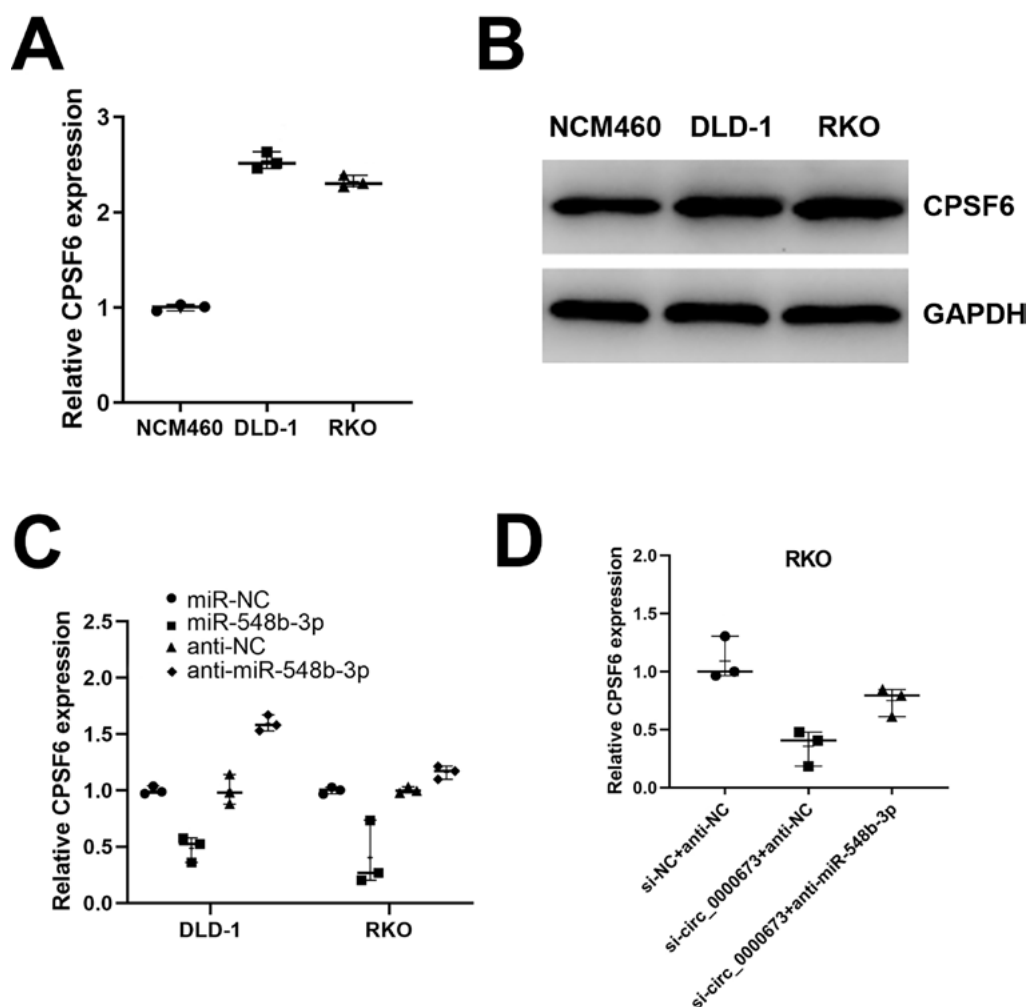


Fig. 8. Circ_0000673 regulated the expression of *CPSF6* by targeting miR-548b-3p in CRC cell lines. A,B. The mRNA and protein levels of *CPSF6* in NCM460, DLD-1 and RKO cells were measured using qPCR and western blot, respectively; C. The expression of *CPSF6* in DLD-1 and RKO cells after transfected with miR-548b-3p mimics or anti-miR-548b-3p was measured with qPCR; D. After co-transfection of si-circ_0000673 and miR-548b-3p inhibitor, the *CPSF6* expression was detected using qPCR. All statistical methods employed in this figure were performed using the Kruskal–Wallis test, followed by the Dunn's test with Bonferroni correction post hoc test

CRC – colorectal cancer;
qPCR – quantitative real-time polymerase chain reaction.

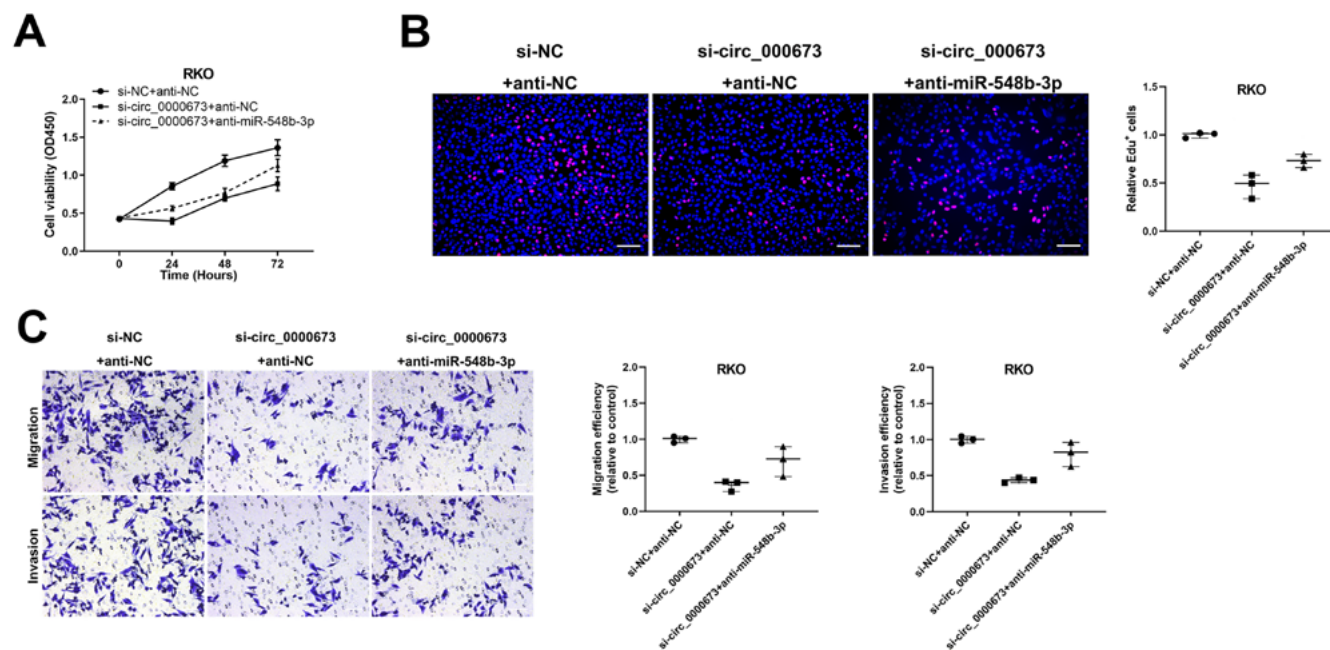


Fig. 9. CCK-8, EdU and transwell assays confirmed that the effects of proliferation, migration and invasion induced by circ_0000673 inhibitor were partly reversed by anti-miR-548b-3p. All statistical methods employed in this figure used the Kruskal–Wallis test as a preliminary analysis, followed by the Bonferroni post hoc test

CCK-8 – Cell Counting Kit-8; EdU – 5-ethynyl-2'-deoxyuridine.

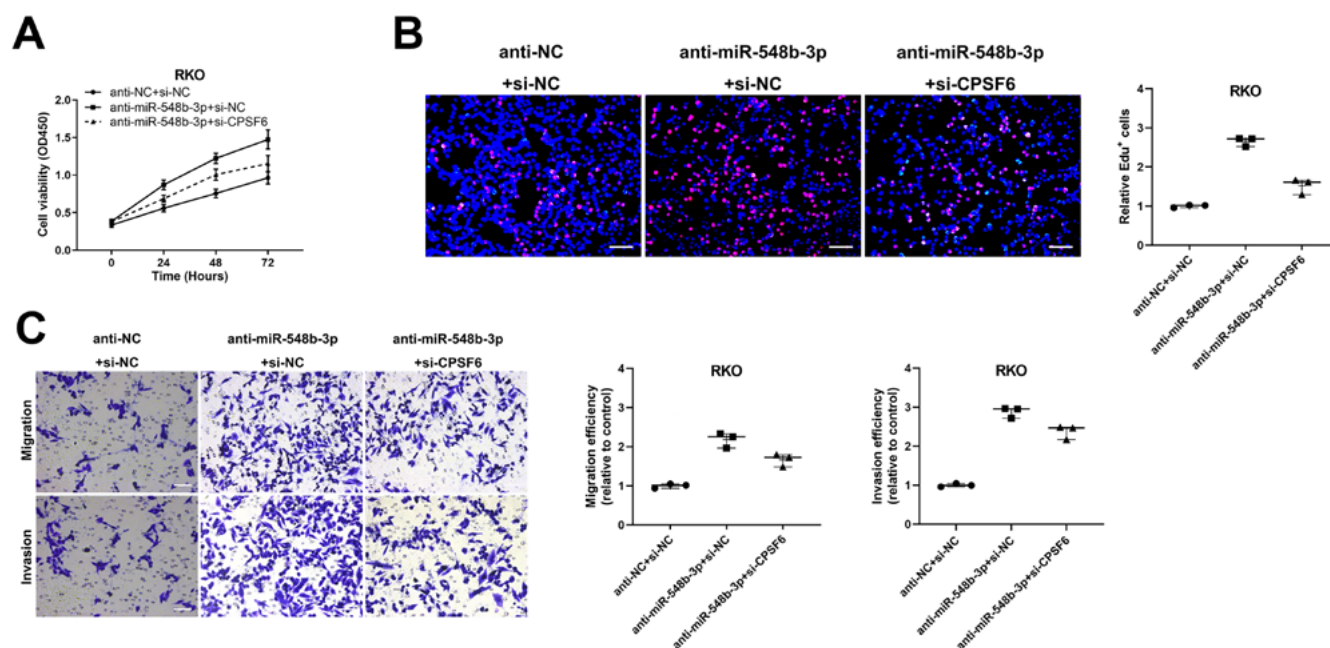


Fig. 10. Silencing *CPSF6* could partially reverse the proliferation, migration and invasion induced by anti-miR-548b-3p in CCK-8, EdU and transwell assays. All statistical methods employed in this figure used the Kruskal–Wallis test as a preliminary analysis, followed by the Bonferroni post hoc test

CCK-8 – Cell Counting Kit-8; EdU – 5-ethynyl-2'-deoxyuridine.

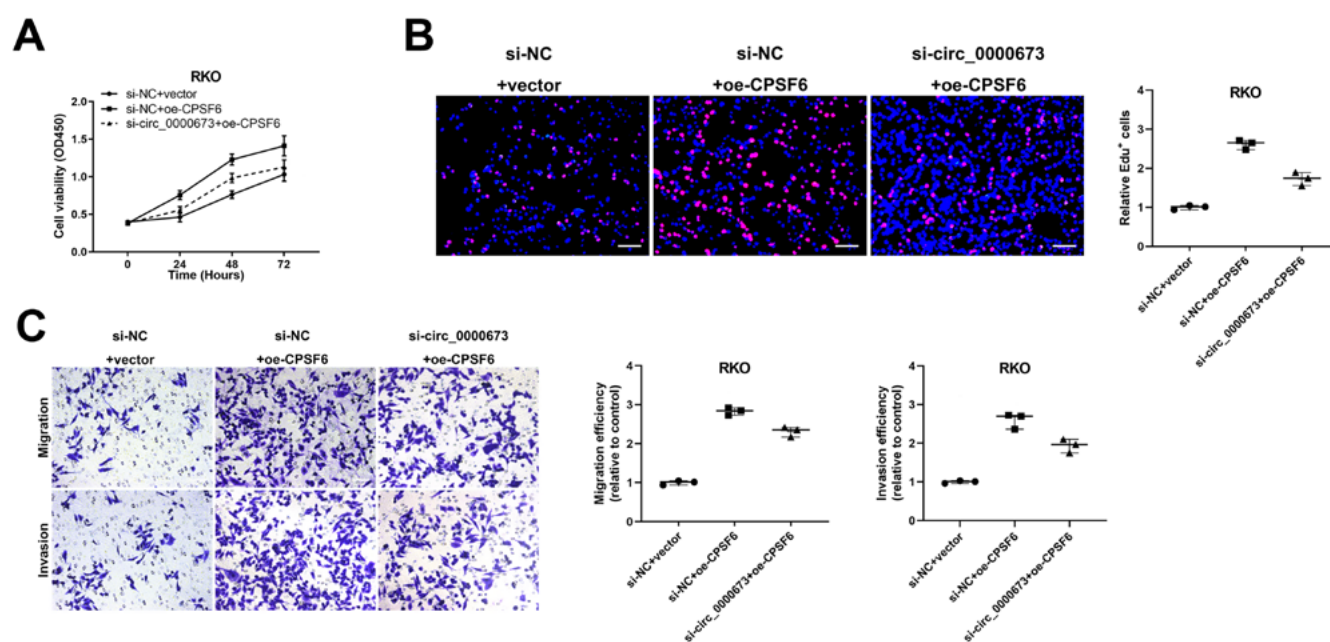


Fig. 11. Restoration of *CPSF6* expression rescued the promotion of proliferation, migration and invasion generated through circ_0000673 inhibition in CCK-8, EdU and transwell, respectively. All statistical methods employed in this figure used the Kruskal–Wallis test as a preliminary analysis, followed by the Bonferroni post hoc test

CCK-8 – Cell Counting Kit-8; EdU – 5-ethynyl-2'-deoxyuridine.

Discussion

The incidence of CRC has remained consistently high over time.¹⁵ Emerging evidence highlights the significant roles that circRNAs play in various human cancers. For instance, circ_0120175 has been shown to promote the proliferation, migration and invasion of lung squamous

cell carcinoma (LSCC) cells through the miR-330-3p/SLC7A11 axis, while concurrently inhibiting apoptosis.¹⁶ Similarly, circ-ZNF609 has been demonstrated to selectively bind to miR-432-5p, leading to increased *LRRC1* expression and facilitating cholangiocarcinoma (CCA).^{17,18} In this study, we have confirmed the elevated expression of circ_0000673 in CRC tissues and cells. Moreover,

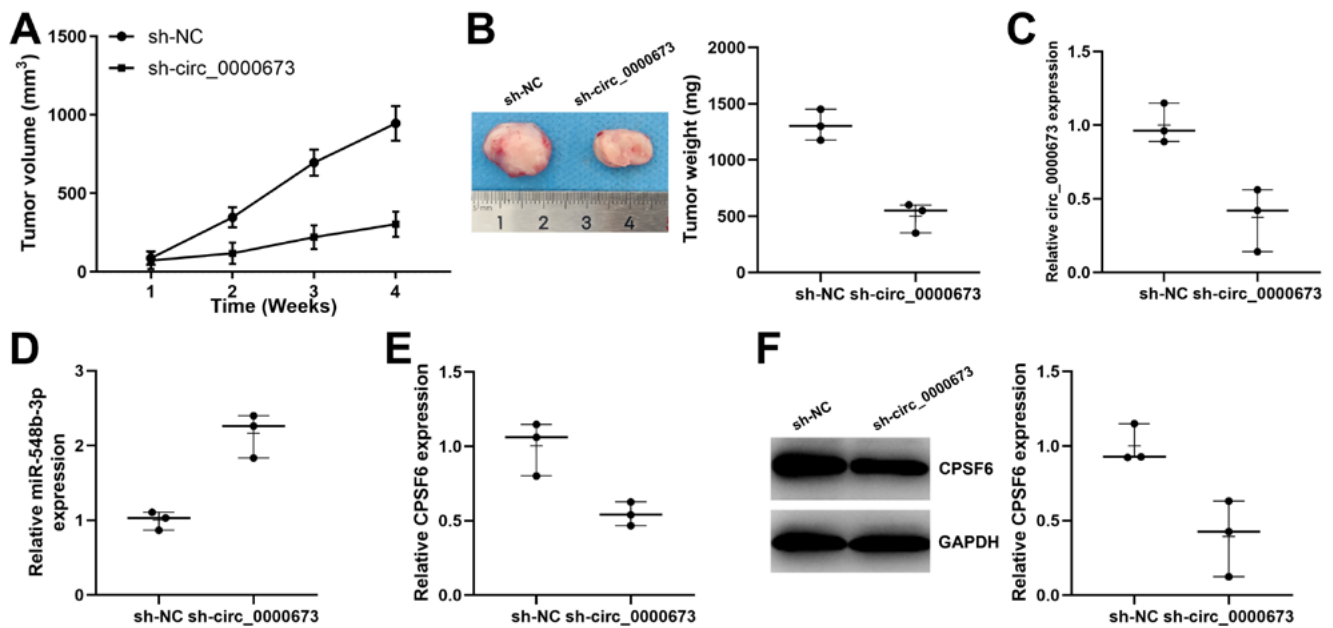


Fig. 12. Downregulated *circ_0000673* inhibited tumor growth in vivo. **A.** Tumor volume was measured every week after injection; **B.** Tumor weight in nude mice at 4 weeks post-injection; **C–E.** The expression of *circ_0000673*, *miR-548b-3p* and *CPSF6* were detected using qPCR in tumor tissue; **F.** The *CPSF6* protein expression in the collected tissues was determined with western blot assay. All statistical analyses employed in this figure were performed using the Mann–Whitney test

qPCR – quantitative real-time polymerase chain reaction.

we observed that high *circ_0000673* expression was associated with shorter OS among CRC patients, and ROC curve analysis suggested that *circ_0000673* might hold potential as a diagnostic biomarker. Notably, the inhibition of *circ_0000673* effectively curtailed the proliferation, migration and invasion of CRC cells while diminishing their stemness. Finally, *circ_0000673* knockdown resulted in the suppression of tumor growth in in vivo experiments. Collectively, these findings underscore the regulatory role of *circ_0000673* as a pro-cancer factor in CRC.

In recent years, accumulating evidence has underscored the pivotal role of circRNAs in gene expression regulation, often achieved through their capacity to sponge miRNAs.¹⁹ In our study, we unveiled that *circ_0000673* functions as a *miR-548b-3p* sponge in CRC cells. Previous research has highlighted the tumor-suppressive effects of elevated *miR-548b-3p* in breast cancer, achieved by inhibiting *MDM2* expression.²⁰ In the context of lung cancer, Wang et al. demonstrated that *miR-548b-3p* acts as an oncogenic suppressor by regulating the PI3K/AKT signaling pathway,²¹ and *miR-548b-3p* suppresses the malignancy of tumor cells by inhibiting the expression of *CIP2A* and *SPI1*.²² Our study has provided conclusive evidence that *miR-548b-3p* is downregulated in CRC tissues and cells. Notably, anti-*miR-548b-3p* partially counteracted the effects of *circ_0000673* silencing on the malignant behaviors of CRC cells. These data collectively suggest that *miR-548b-3p* plays a tumor-suppressive role in CRC, whereas *circ_0000673* functions as an accelerator of CRC progression by sponging *miR-548b-3p*.

Our study uncovers the role of *CPSF6* as a target gene of *miR-548b-3p* in CRC cells. In gastric cancer, *CPSF6* has been shown to negatively regulate *VHL* expression through alternative polyadenylation (APA), and the *VHL* short 3'UTR heterodimer induced apoptosis and hindered the growth of gastric cancer cells.²³ Similarly, *CPSF6* has been implicated in the progression of hepatocellular carcinoma (HCC) by upregulating *NQO1* expression through APA.²⁴ In a study by Liu et al., *CPSF6* was found to inhibit *BTG2* expression, promote glycolysis and suppress apoptosis in HCC cells.²⁵ In our investigation, we observed an upregulation of *CPSF6* in CRC tissues and cells, and the increased *CPSF6* levels counteracted the inhibitory effects of *miR-548b-3p* overexpression and si-*circ_0000673* on the malignant behavior of CRC cells. These findings collectively suggest that *CPSF6* plays an oncogenic role in CRC. Therefore, we conclude that *circ_0000673* regulates the progression of CRC by sponging *miR-548b-3p* to modulate the expression of *CPSF6*.

Limitations

Our study revealed the function and mechanism of *circ_0000673* in CRC development. However, we did not investigate further the upstream regulatory mechanisms of *circ_0000673*, such as whether there is a strongly associated transcription factor causing abnormal expression of *circ_0000673* in CRC. Furthermore, studies related to the clinical application of *circ_0000673* have not been performed, including those examining its relationship with tumor drug resistance capacity.

Conclusions

To sum up, circ_0000673 assumes a tumor-promoting role within the context of CRC, actively driving its progression by orchestrating the miR-548b-3p/CPSF6 axis. These findings propose that circ_0000673 holds potential as a promising target for the diagnosis and treatment of CRC in clinical practice.

Supplementary data

The Supplementary materials are available at <https://doi.org/10.5281/zenodo.10867861>. The package includes the following files:

Supplementary Table 1. Primers used in this study.

Supplementary Table 2. Statistical methods and test results used.

Data availability

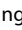
The datasets generated and/or analyzed during the current study are available from the corresponding author on reasonable request.


Consent for publication

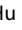
Not applicable.


ORCID iDs


Shuang Li  <https://orcid.org/0009-0003-3287-9021>

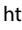
Tuoyun Yang  <https://orcid.org/0009-0006-8807-5550>

Lu Liu  <https://orcid.org/0009-0004-5226-868X>

Baorong Hu  <https://orcid.org/0009-0006-9880-7428>

Xi Chen  <https://orcid.org/0009-0005-5205-8970>

Wenting Zhao  <https://orcid.org/0009-0006-8326-0837>

Xin Hai  <https://orcid.org/0009-0002-4971-0727>

References

1. Thanikachalam K, Khan G. Colorectal cancer and nutrition. *Nutrients*. 2019;11(1):164. doi:10.3390/nu11010164
2. Jin K, Ren C, Liu Y, Lan H, Wang Z. An update on colorectal cancer micro-environment, epigenetic and immunotherapy. *Int Immunopharmacol*. 2020;89:107041. doi:10.1016/j.intimp.2020.107041
3. Ruan J, Zhang P, Zhang Q, et al. Colorectal cancer inhibitory properties of polysaccharides and their molecular mechanisms: A review. *Int J Biol Macromol*. 2023;238:124165. doi:10.1016/j.ijbiomac.2023.124165
4. Zielińska A, Włodarczyk M, Makaro A, Sałaga M, Fichna J. Management of pain in colorectal cancer patients. *Crit Rev Oncol Hematol*. 2021;157:103122. doi:10.1016/j.critrevonc.2020.103122
5. Lu Y, Liu Q, Fu B, Li P, Xu W. Label-free MIP-SERS biosensor for sensitive detection of colorectal cancer biomarker. *Talanta*. 2023;258:124461. doi:10.1016/j.talanta.2023.124461
6. Gao J, Chen X, Shan C, Wang Y, Li P, Shao K. Autophagy in cardiovascular diseases: Role of noncoding RNAs. *Mol Ther Nucleic Acids*. 2021;23:101–118. doi:10.1016/j.omtn.2020.10.039
7. Chia W, Liu J, Huang YG, Zhang C. A circular RNA derived from DAB1 promotes cell proliferation and osteogenic differentiation of BMSCs via RBPJ/DAB1 axis. *Cell Death Dis*. 2020;11(5):372. doi:10.1038/s41419-020-2572-3
8. Zeng W, Guo M, Yao L, Deng Z. Circular RNA hsa_circ_0033144 (CircB-CL11B) regulates oral squamous cell carcinoma progression via the miR-579/LASP1 axis. *Bioengineered*. 2021;12(1):4111–4122. doi:10.1080/21655979.2021.1953214
9. Xu P, Xu X, Wu X, et al. CircTMC5 promotes gastric cancer progression and metastasis by targeting miR-361-3p/RABL6. *Gastric Cancer*. 2022;25(1):64–82. doi:10.1007/s10120-021-01220-6
10. Kumar S, Gonzalez EA, Rameshwar P, Etchegaray JP. Non-coding RNAs as mediators of epigenetic changes in malignancies. *Cancers (Basel)*. 2020;12(12):3657. doi:10.3390/cancers12123657
11. Yang H, Zhao M, Zhao L, Li P, Duan Y, Li G. CircRNA BIRC6 promotes non-small cell lung cancer cell progression by sponging microRNA-145. *Cell Oncol*. 2020;43(3):477–488. doi:10.1007/s13402-020-00503-x
12. Jiang Z, Hu H, Hu W, et al. Circ-RNF121 regulates tumor progression and glucose metabolism by miR-1224-5p/FOXO1 axis in colorectal cancer. *Cancer Cell Int*. 2021;21(1):596. doi:10.1186/s12935-021-02290-3
13. An Y, Xu B, Yan G, Wang N, Yang Z, Sun M. YAP derived circ-LECRC functions as a “brake signal” to suppress hyperactivation of oncogenic YAP signalling in colorectal cancer. *Cancer Lett*. 2022;532:215589. doi:10.1016/j.canlet.2022.215589
14. Zhao Y, Wang W, Guan C, et al. Long noncoding RNA HOTAIRM1 in human cancers. *Clin Chim Acta*. 2020;511:255–259. doi:10.1016/j.cca.2020.10.011
15. Nair HG, Jurkiewicz A, Graczyk D. Inhibition of RNA polymerase III augments the anti-cancer properties of TNFα. *Cancers (Basel)*. 2023;15(5):1495. doi:10.3390/cancers15051495
16. Wen X, Han W, Liu C. hsa_circ_0017842 acts as a competing endogenous RNA to enhance the malignancy of gastric cancer. *Adv Clin Exp Med*. 2023;32(7):803–812. doi:10.17219/acem/158484
17. Liu L, Wang H, Yu S, et al. An update on the roles of circRNA-ZFR in human malignant tumors. *Front Cell Dev Biol*. 2022;9:806181. doi:10.3389/fcell.2021.806181
18. Guan C, Liu L, Zhao Y, et al. YY1 and eIF4A3 are mediators of the cell proliferation, migration and invasion in cholangiocarcinoma promoted by circ-ZNF609 by targeting miR-432-5p to regulate LRRC1. *Aging*. 2021;13(23):25195–25212. doi:10.18632/aging.203735
19. Liu P, Wang J, Du W, Chen L. LncRNA SNHG12 promotes proliferation and migration of hepatic progenitor cells via the Wnt/β-catenin pathway. *Adv Clin Exp Med*. 2023;32(9):1017–1027. doi:10.17219/acem/159475
20. Sha MX, Huang XW, Yin Q. MiR-548b-3p inhibits proliferation and migration of breast cancer cells by targeting MDM2. *Eur Rev Med Pharmacol Sci*. 2020;24(6):3105–3112. doi:10.26355/eurrev_202003_20675
21. Wang Z, Wu X, Hou X, et al. miR-548b-3p functions as a tumor suppressor in lung cancer. *Lasers Med Sci*. 2020;35(4):833–839. doi:10.1007/s10103-019-02865-7
22. Lin L, Wang Y. miR-548b-3p regulates proliferation, apoptosis, and mitochondrial function by targeting CIP2A in hepatocellular carcinoma. *BioMed Res Int*. 2018;2018:7385426. doi:10.1155/2018/7385426
23. Shi X, Ding K, Zhao Q, et al. Suppression of CPSF6 enhances apoptosis through alternative polyadenylation-mediated shortening of the VHL 3'UTR in gastric cancer cells. *Front Genet*. 2021;12:707644. doi:10.3389/fgene.2021.707644
24. Tan S, Zhang M, Shi X, et al. CPSF6 links alternative polyadenylation to metabolism adaption in hepatocellular carcinoma progression. *J Exp Clin Cancer Res*. 2021;40(1):85. doi:10.1186/s13046-021-01884-z
25. Liu Y, Zou H, Xie Q, Zou L, Kong R, Mao B. Ribonucleic acid-binding protein CPSF6 promotes glycolysis and suppresses apoptosis in hepatocellular carcinoma cells by inhibiting the BTG2 expression. *Biomed End Online*. 2021;20(1):67. doi:10.1186/s12938-021-00903-6